applied sciences

MDPI

Article

Thermo-Responsive Shape-Memory Effect and Surface Features in Polycarbonate (PC)

Xue Lian Wu [1], Tao Xi Wang [2], Wei Min Huang [2,*] and Yong Zhao [3]

1 School of Mechanical Engineering, Jiangsu University, 301 Xuefu Road, Zhenjiang 212013, China; ujswxl@163.com
2 School of Mechanical and Aerospace Engineering, Nanyang Technological University, 50 Nanyang Avenue, Singapore 639798, Singapore; WA0003XI@e.ntu.edu.sg
3 School of Chemistry and Chemical Engineering, Jiangsu University, 301 Xuefu Road, Zhenjiang 212013, China; yn.zhao2@gmail.com
* Correspondence: mwmhuang@ntu.edu.sg; Tel.: +65-6790-4859; Fax: 65-6792-4062

Received: 9 July 2017; Accepted: 16 August 2017; Published: 17 August 2017

Abstract: The influence of programming strain and temperature on the shape memory effect and surface morphology in programmed polycarbonate (PC) samples via uni-axial stretching is investigated. It is found that the samples programmed at around the glass transition start temperature not only have micro-cracks on their surface, but also show a necking phenomenon. Furthermore, the surface of the necked area is concave, but the surface of the non-necked area is convex. On the other hand, despite the samples programmed at high temperatures being able to deform in a uniform manner at macroscopic scale, their surfaces are still uneven, either concave or convex. While the samples programmed at low temperatures are able to achieve full shape recovery, stretching at higher temperatures over the glass transition range to a higher strain may result in non-recoverable deformation.

Keywords: polycarbonate; shape memory effect; necking; crack; shape recovery; concave; convex

1. Introduction

The ability to return the original shape of a material, but only at the presence of the right stimulus, such as heat, light and chemicals, is called the shape memory effect (SME) [1–3]. Consequently, the materials with SME are known as shape memory materials (SMM) at present. The family of SMM has expanded dramatically in recent years, in particular, to include many types of polymeric materials. According to, for instance [4], most polymers are naturally heating/chemo-responsive SMM. In addition to continuous efforts to develop new SMMs [5–16], the SME in many engineering polymers has been systematically characterized and gradually utilized in some engineering applications [17–27].

Polycarbonate (PC) is a widely used thermoplastic engineering polymer particularly due to its high toughness, good flame resistance and durability. PC is a typical linear co-polymer with carbonate as a repeating unit. Well-documented experimental results of its standard properties are now available in the literature. Its heating-responsive SME as revealed in Figure 1 inspires us to further explore its shape memory behavior for potential engineering applications in the future.

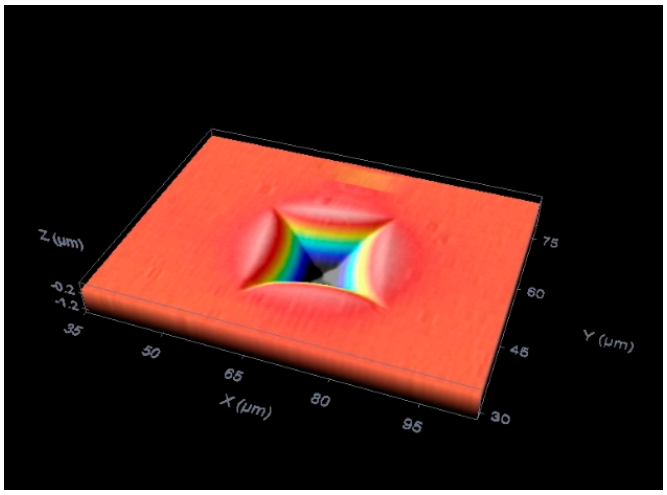

(**a1**)

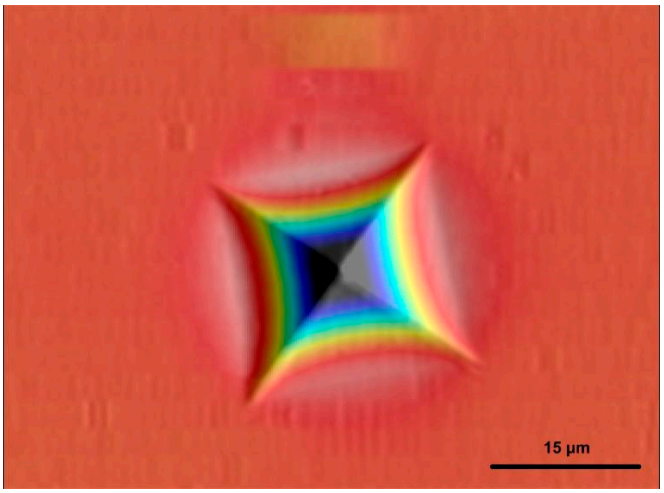

(**a2**)

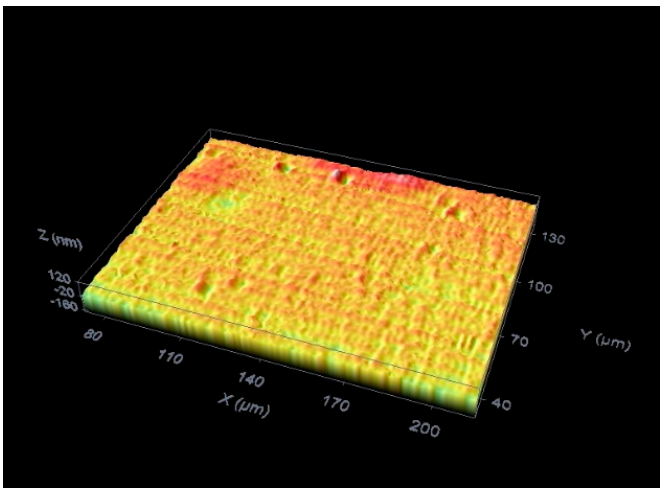

(**b1**)

Figure 1. *Cont*.

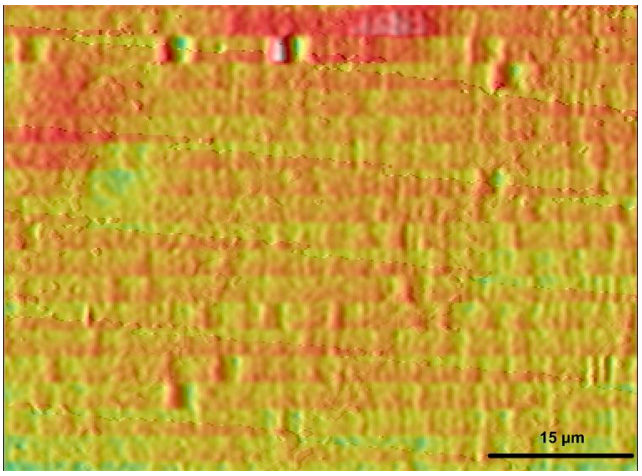

(**b2**)

Figure 1. Heating-responsive shape recovery after indentation at room temperature. (**a1**,**a2**) are 3D view and top view of the indent, respectively; (**b1**,**b2**) are 3D view and top view of the surface after heating, respectively. The scale bar in the subfigures of the right column is 15 μm.

In this paper, the influence of programming temperature and programming strain via uni-axial tension on the heating-responsive SME in a commercial PC is systematically investigated. In addition, since PC is a commonly used optical polymer, the surface features of programmed samples are examined at both macro and micro scales.

The shape recovery in this PC is not due to relaxation/creeping, since it is able to maintain the temporary shape unless heat, which is used in this study as the stimulus, is applied. Thus, it is important to characterize its shape fixation ratio and shape recovery ratio under different processing parameters.

2. Material, Thermal Analysis and Samples Preparation

PC sheets with a thickness of 2.0 mm were bought from Polyfluo Asia Private Limited, Singapore. Some small pieces were cut out of the as-received PC sheet for thermal analysis.

Thermogravimetric analysis (TGA) (TGA 2950, Surplus Solutions Inc., Woonsocket, RI, USA) was conducted from 25 °C to 850 °C at a ramp rate of 10 °C/min. According to Figure 2, there is virtually no weight loss before 400 °C, which confirms high thermal stability of this PC. The derivative weight (%/°C) is automatically worked out by the program of the TGA machine.

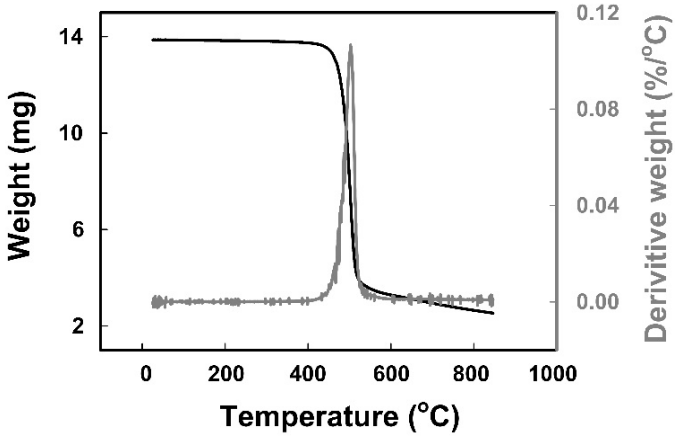

Figure 2. Typical thermogravimetric analysis (TGA) result. Black line: weight; grey line: derivative weight.

Differential scanning calorimetric (DSC) (DSC Q200, Coppell, TX, USA) tests were carried out between 25 °C and 380 °C at a ramp rate of 10 °C/min for two cycles. As revealed in Figure 3 (the result of the second cycle), the glass transition of this PC occurs between 130 °C and 150 °C, and 142 °C may be defined as its glass transition temperature (T_g).

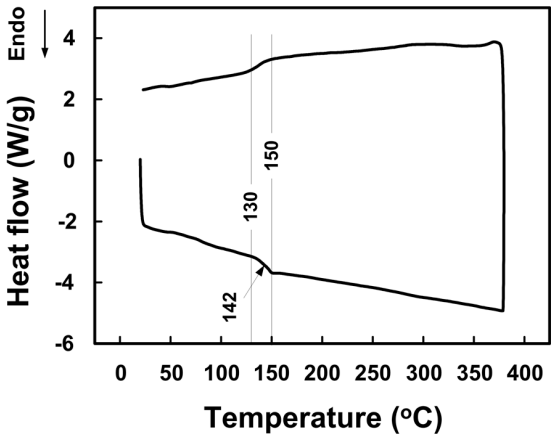

Figure 3. Typical differential scanning calorimetric (DSC) result (the second cycle).

Dog-bone shaped samples (refer to Figure 4 for dimensions) for uni-axial tensile test were cut out from the PC sheets.

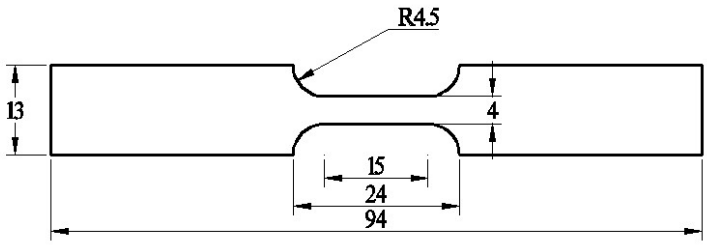

Figure 4. Dimensions of dog-bone shaped sample (according to ASTM D638, Type IV).

3. Characterization of Heating-Responsive SME

A standard thermo-responsive SME cycle, programmed by means of, for instance, uni-axial tension in this study, includes two processes, namely programming and shape recovery, with three major steps as illustrated in Figure 5 [28].

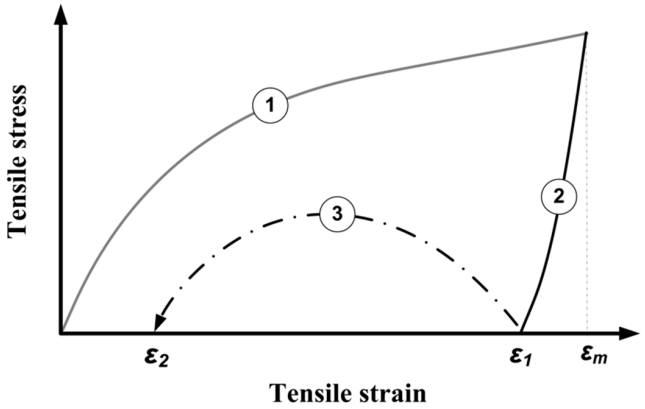

Figure 5. Illustration of stress versus strain relationship in a standard shape memory effect (SME) cycle. The numbers inside of the circles are meant for the steps.

Step 1 Loading: at a prescribed programming temperature, stretching the sample to the required maximum strain of ε_m at a prescribed strain rate;

Step 2 Unloading: after cooling the sample back to the room temperature (if the programming temperature is above the room temperature), the sample is unloaded at the same strain rate as that in loading. For materials without significant relaxation/creeping at room temperature, as observed in this PC, the residual strain after unloading may be defined as ε_1. This ends the first process of programming;

Step 3 Heating: the programmed sample is heated and the remaining strain after heating is defined as ε_2. This ends the second process of shape recovery.

The actual heating recovery strain can be estimated as $(\varepsilon_1 - \varepsilon_2)$, and hence, the shape fixity ratio (R_f) and shape recovery ratio (R_r) may be defined as [19],

$$R_f = \frac{\varepsilon_1}{\varepsilon_m} \tag{1}$$

$$R_r = \frac{\varepsilon_1 - \varepsilon_2}{\varepsilon_1} \tag{2}$$

A series of tensile tests were conducted on dog-bone shaped samples at different programming temperatures to different maximum programming strains using an Instron 5565 (with a temperature controllable chamber). To be more precise, the actual temperature during testing was monitored using a thermal couple attached to the tested sample. A constant strain rate of 10^{-3}/s was applied in both loading and unloading in all tensile tests in the course of this study.

Unless otherwise stated, the stress and strain mentioned here are meant for engineering stress and engineering strain.

Pre-stretching was conducted in two different manners, one is at room temperature (about 25 °C) for tests with the maximum programming strains of 5%, 10%, 15%, 20% and 25%, respectively, and the other is at high temperatures (around the glass transition range) for three maximum programming strains of 20%, 30% and 100%, respectively. After programming, thermally (heating) induced shape recovery test was conducted at 180 °C for samples programmed at room temperature, or at previous programming temperature and then at 180 °C for samples programmed at high temperatures. Since the applied maximum programming strain is 5% or more, thermal strain is relatively smaller and thus, it is ignored herein.

3.1. Influence of Maximum Programming Strain (Room Temperature Programming)

To investigate the influence of the maximum programming strain on the SME at room temperature, some samples were pre-stretched at room temperature to five maximum tensile strains (ε_m) (namely, 5%, 10%, 15%, 20% and 25%) and then unloaded. Note that it was found that over 25% straining at room temperature may cause fracture of the sample.

Typical strain versus stress relationships are presented in Figure 6. As we can see, in the cases of 5% and 10% programming strains, the samples experience mainly elastic deformation. With the increase in maximum programming strain, more quasi-plastic strain is built up, and thus more residual strain is observed after unloading. Figure 7 (black symbols) presents the relationship of R_f versus the maximum tensile programming strain. As we can see, when the maximum programming strain increases from 5% to 10%, R_f increases slightly from 3% to 6.5%. Upon further increasing of ε_m, R_f increases significantly. Over 60% is observed at 25% maximum programming strain.

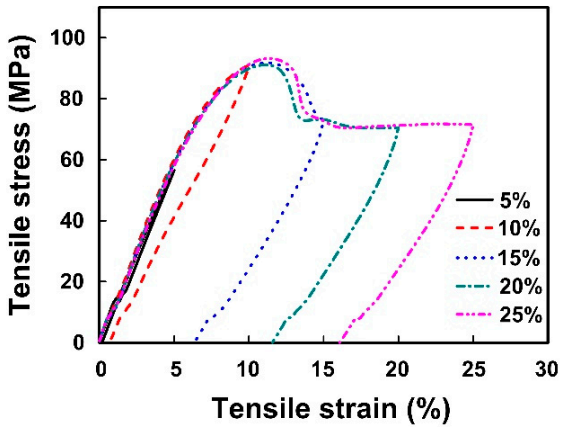

Figure 6. Typical stress versus strain relationships in uni-axial tension to five different programming strains at room temperature, and then followed by unloading.

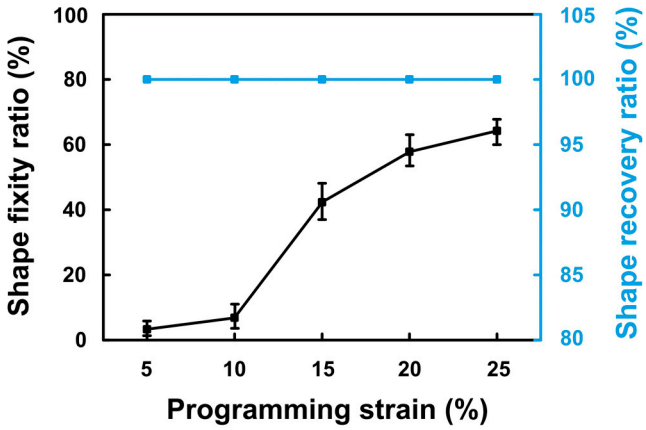

Figure 7. Shape fixity ratio and shape recovery ratio upon heating to 180 °C versus programming strain relationships for samples programmed at room temperature.

After programming, the samples were heated to 180 °C, which is about 40 °C higher than the T_g of this material according to the DSC result reported in Figure 3. According to Figure 7 (blue symbols), all samples are virtually able to fully recover their original shape.

3.2. Influence of Programming Temperature and Strain (High Temperature Programming)

3.2.1. Shape Fixity Ratio

A few series of tests were conducted at different high programming temperatures to different programming strains. Typical strain versus stress relationships of these tests are presented in Figure 8 for programming strains of 30% and 100%. Note that in each test, upon reaching the prescribed maximum programming strain, cooling to room temperature was followed before unloading at the same speed as in loading.

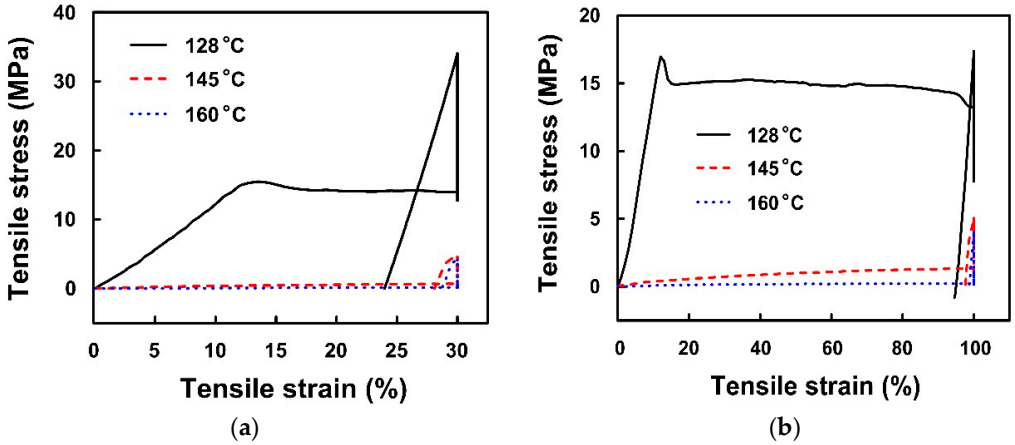

Figure 8. Typical stress versus strain curves in uni-axial tension at different temperatures to maximum programming strains of 30% (**a**) and 100% (**b**) and then unloading after cooling to room temperature.

As shown in Figure 8, despite some discrepancy, the stress vs. strain relationships of the samples with both 30% and 100% maximum programming strains share the same trend. It is obvious that with the increase in programming temperature, the material shows less resistance to deformation. The yield strength is about 16 MPa in samples programmed to both strains of 30% and 100% at 128 °C (which is a temperature slightly below the glass transition start temperature, 130 °C, according to Figure 3), while for the samples programmed at 145 °C (slightly below the glass transition finish temperature, 150 °C) and at 160 °C (above the glass transition finish temperature, 150 °C), there is no clear yield point and the corresponding strength is much lower.

When compared with the yield stress of around 90 MPa at room temperature in Figure 6, the yield stress of about 16 MPa at 128 °C (Figure 8) is significantly lower. Hence, it can be concluded that part of the material is already softened at 128 °C.

Figure 9 presents the relationship of shape fixity ratio (R_f) versus programming temperature for 20%, 30% and 100% maximum programming strains. Same as those in many other engineering polymers reported in the literature [17–19], R_f of this PC increases with not only the increase in the maximum programming strain, but also the increase in programming temperature.

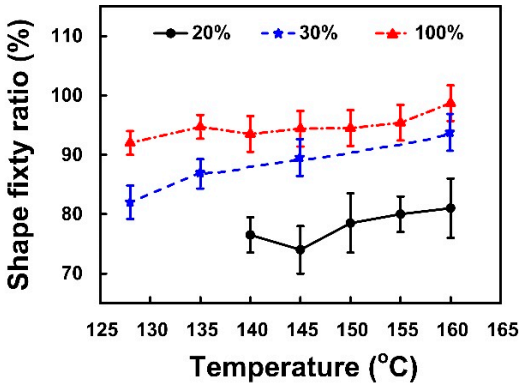

Figure 9. Shape fixity ratio (R_f) against programming temperature with three different maximum programming strains.

3.2.2. Shape Recovery Ratio

Heating-responsive shape recovery test was conducted in two steps. In the first step, the sample was heated to the previous programming temperature for 20 min. In the second step, the sample was

further heated to 180 °C for 20 min. Figure 10 presents R_r upon two-step heating in samples with maximum programming strains of 20%, 30% and 100%.

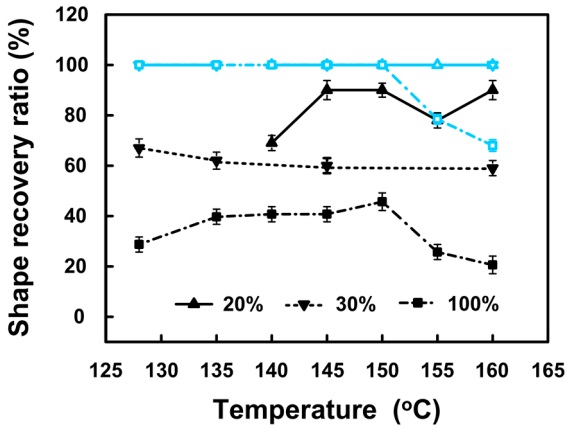

Figure 10. Shape recovery ratio (R_r) as a function of the programming temperature and programming strain. Black line: upon heating to the programming temperature; blue line: upon further heating to 180 °C.

As we can see, for samples programmed to 20% maximum programming strain, significant recovery is observed upon heating to the previous programming temperature in all samples, as the corresponding shape recovery ratio ranges from 67 to 89% and the average is over 80%. Upon further heating to 180 °C, all of them reach 100% shape recovery.

For samples programmed to 30% maximum programming strain, upon heating to the previous programming temperature the shape recovery ratio is lower than those samples with 20% maximum programming strain, only around 60% to 70%. A higher programming temperature seemingly reduces the shape recovery ratio slightly. However, 100% shape recovery is still obtained upon further heating to 180 °C in all samples.

For samples programmed to 100% maximum programming strain, the shape recovery ratio does not monotonically increase or decrease with the increase in programming temperature as that in samples programmed with 30% programming strain. It increases with the increase in programming temperature till 150 °C, in which the corresponding shape recovery ratio is about 40%, and then decreases if the programming temperature is higher. Different from those programmed to 20% and 30% strains, upon further heating to 180 °C, full shape recovery is only observed in samples programmed at 150 °C or below. A higher programming temperature over 150 °C results in less shape recovery. According to [4], this is most likely due to permanent plastic deformation in the elastic component/chain/segment of the PC at high programming strain and high programming temperature.

4. Characterization of Surface Features

In this section, we present the surface features of the programmed samples. Experimental results are summarized in Figure 11, and the details are discussed in the following subsections. Four different programming temperatures were selected to carry out a series of uni-axial tensile tests on the same dog-bone shaped samples as used in Section 3. Refer to the top subfigure in Figure 11, which schematically illustrates the DSC result of this PC. While 128 °C is supposed to be slightly lower than the glass transition start temperature of 130 °C, the other two programming temperatures of 135 °C and 145 °C are slightly higher than the glass transition start temperature and slightly below the glass transition finish temperature, respectively. The forth programming temperature of 160 °C is well above the glass transition finish temperature. Two different maximum strains of 30% (small strain) and 100% (large strain) were applied to investigate the influence of the actual magnitude of the applied programming strain.

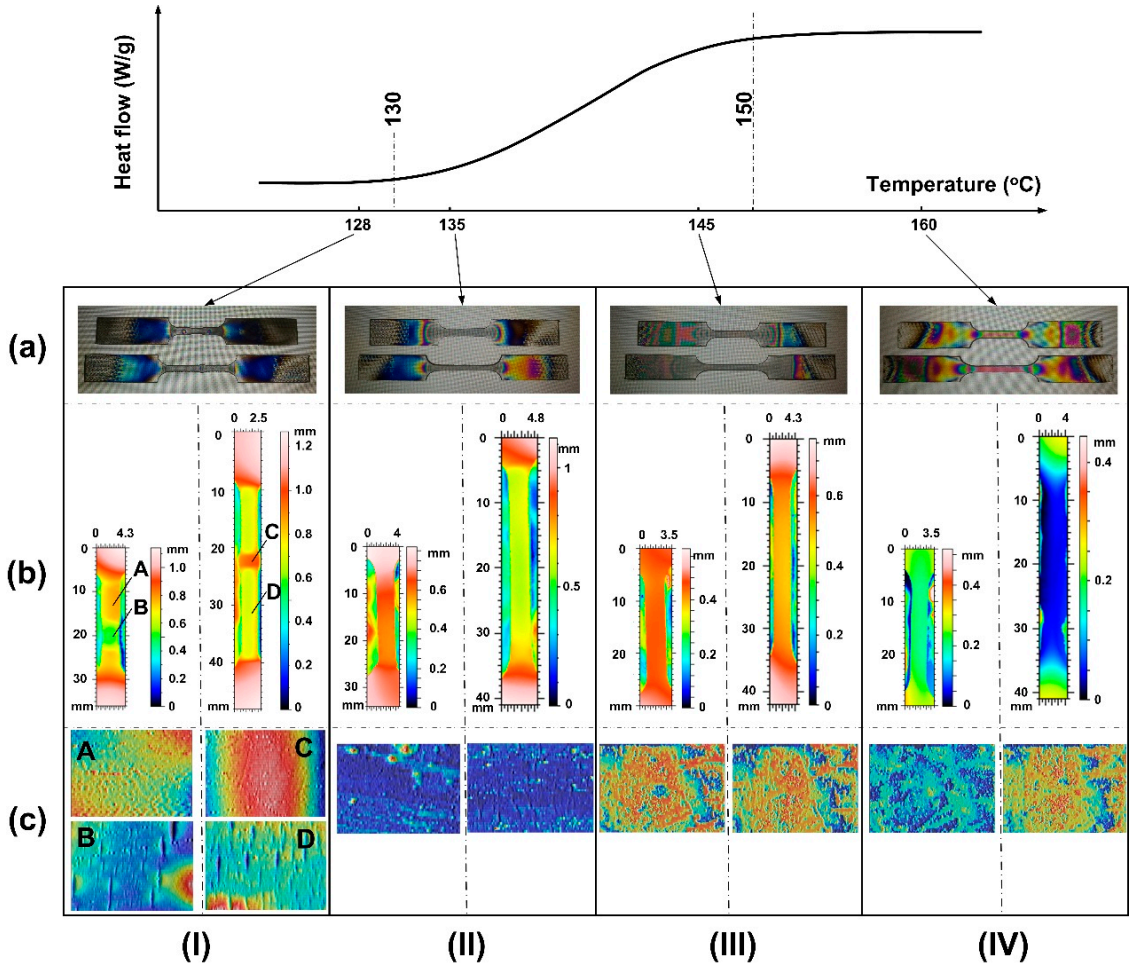

Figure 11. Summary of samples programmed to 30% and 100% strains at four temperatures of 128 °C (**I**); 135 °C (**II**); 145 °C (**III**) and 160 °C (**IV**). Top-subfigure: illustration of DSC curve. (**a**) Image of photo-elastic effect (top sample: 30% strain; bottom sample: 100% strain); (**b**) macro-scale 3D scanning result of sample surface (by Taylor Scanner); (**c**) micro-scale 3D scanning of zoom-in surface (area: 140 × 100 μm) (by PLμ Confocal Imaging Profiler).

The programmed samples were examined at room temperature to show their overall shape change via the photo-elastic effect (Figure 11a), and 3D surface morphologies at both macro-scale (Figure 11b) and micro-scale (Figure 11c).

4.1. Shape Change and Residual Stress

The photo-elastic effect was utilized to examine the overall shape change and the distribution of residual stress in the samples after programming. The programmed samples were placed on the top of the screen of a notebook computer, which provides a polarized light source. The photos of the programmed samples were taken behind a polaroid.

As shown in Figure 12, within the gauge length part, only the samples programmed at 128 °C show necking phenomenon. Correspondingly, in its stress versus strain curve, we can see apparent yielding point followed by stress plateau (Figure 8). Furthermore, we can see remarkable color variation in the transition area from the necked part to the non-necked part, which indicates high residual stress within this area. In other samples programmed at higher temperatures, the deformation is seemingly uniform within the gauge length part, so that there is not much singificant color variation in this part.

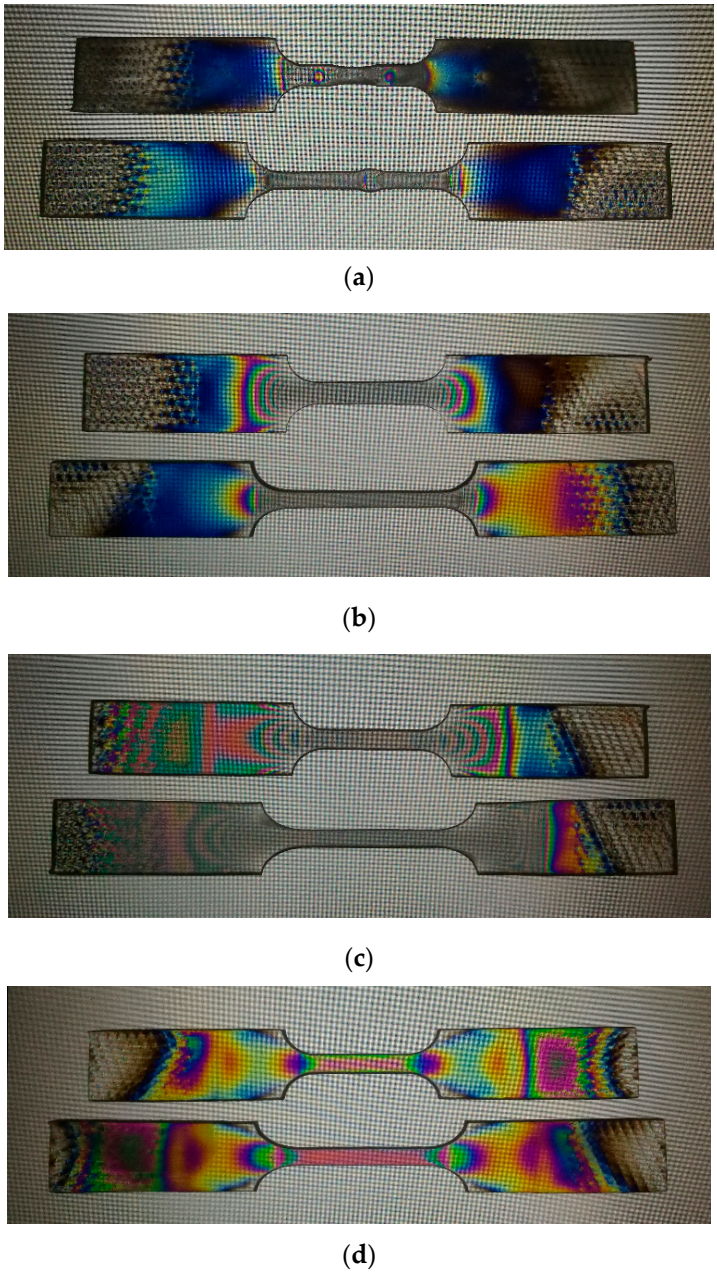

Figure 12. Images of the photo-elastic effect in samples programmed to two maximum programming strains of 30% (**top**) and 100% (**bottom**) at 128 °C (**a**); 135 °C (**b**); 145 °C (**c**) and 160 °C (**d**).

4.2. Surface Morphology

The 3D surfaces of the programmed samples within the gauge length part were further investigated using a Taylor Hobson Scan 150 Measuring System.

Figure 13 presents the scanning result in 2D (a) and 3D (b) of the sample stretched at 128 °C to 30% programming strain. Surface profile of three lines marked in Figure 13a is plotted in Figure 13c (cross-section) and Figure 13d (gauge length direction). Figure 14 is the scanning result of the sample stretched at the same temperature, but to 100% programming strain.

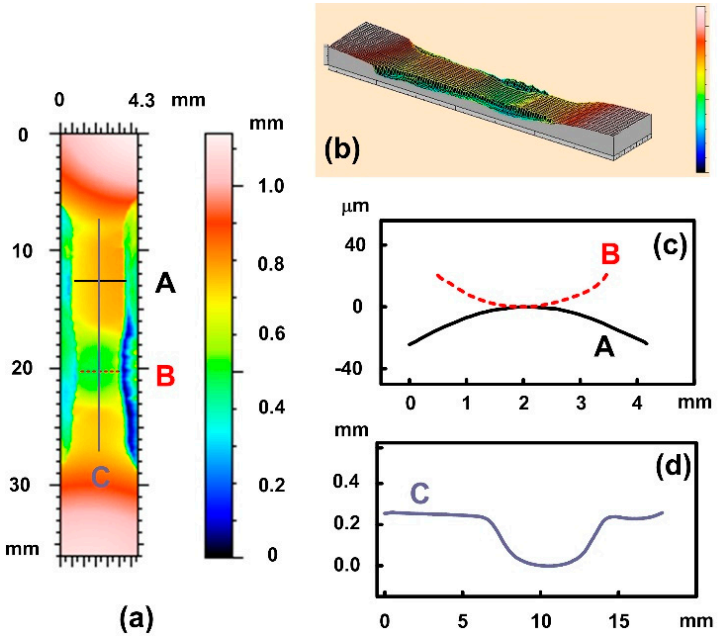

Figure 13. Surface morphology of sample programmed to 30% strain at 128 °C. (**a**) Top view; (**b**) 3D view; (**c**) surface profile of lines A (non-necked area) and B (naked area) as marked in (**a**); (**d**) profile of line C (throughout the gauge length of the sample) as marked in (**a**).

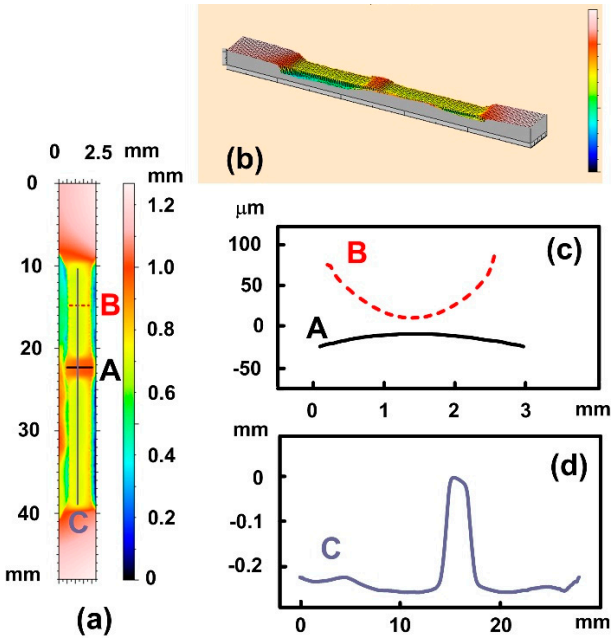

Figure 14. Surface morphology of sample programmed to 100% strain at 128 °C. (**a**) Top view; (**b**) 3D view; (**c**) cross-profile of lines A (non-necked area) and B (naked area) as marked in (**a**); (**d**) profile of line C (throughout the gauge length of the sample) as marked in (**a**).

A close look as presented in Figure 15 reveals that the surface of non-necked area is convex, while the surface of the necked area is concave. Same convex/concave results are obtained in the backsides of these samples as well. The lens effect is examined in Figure 16, in which a sample programmed to 100% strains at 128 °C is uesd. Depending on the actual distance between the sample and a piece of

paper, the printed grid on the paper may be blur or clear. Since the naked area is concave in the vertical direction, the clear grid appears to be narrower in the veritical direction as shown in Figure 16b.

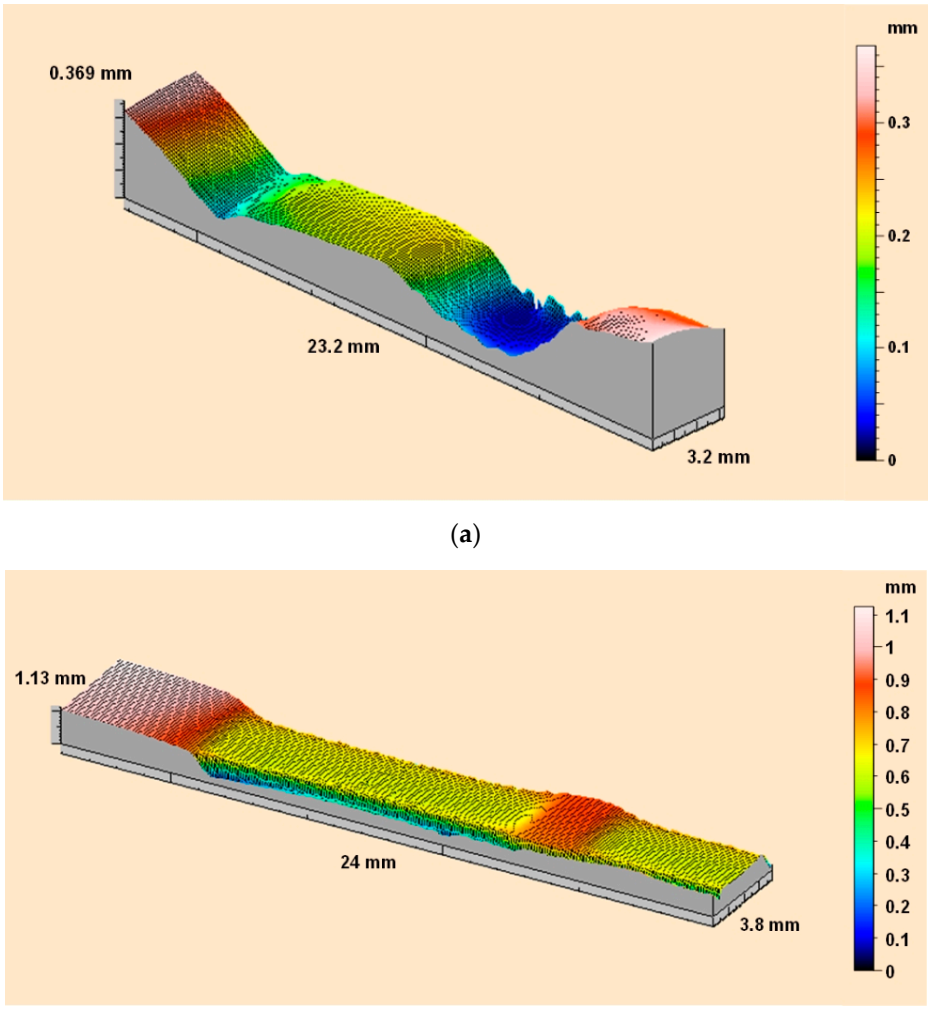

Figure 15. Concave and convex surfaces in naked and non-naked areas in 30% (**a**) and 100% (**b**) stretched samples.

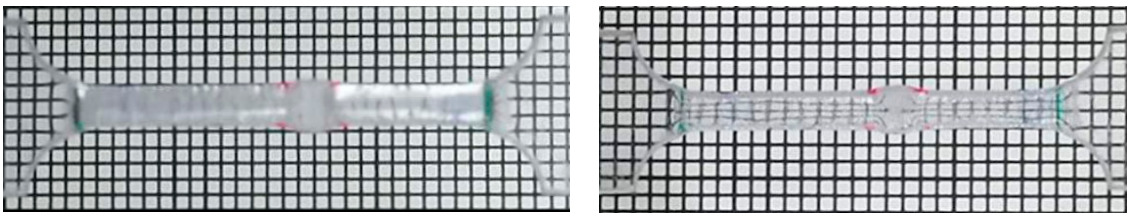

Figure 16. Lens effect in the sample programmed to 100% strain at 128 °C. (**a**) 56.5 mm above the grid paper (blur); (**b**) 13 mm above the grid paper (clear).

The samples tested at 135 °C and above do not show necking phenomenon and thus the deformation within the gauge length part should be uniform. However, typical cross-sections of these samples presented in Figure 17 reveal convex or concave surface in these samples. In terms of magnitude of the curved surface, only the sample stretched to 100% at 135 °C is comparable to the

naked areas of the samples stretched at 128 °C. The rest is only about 10 μm or less, which under normal situation, may be largely ignored as the width of the samples is at millimeter scale. However, for optical applications, it must be considered.

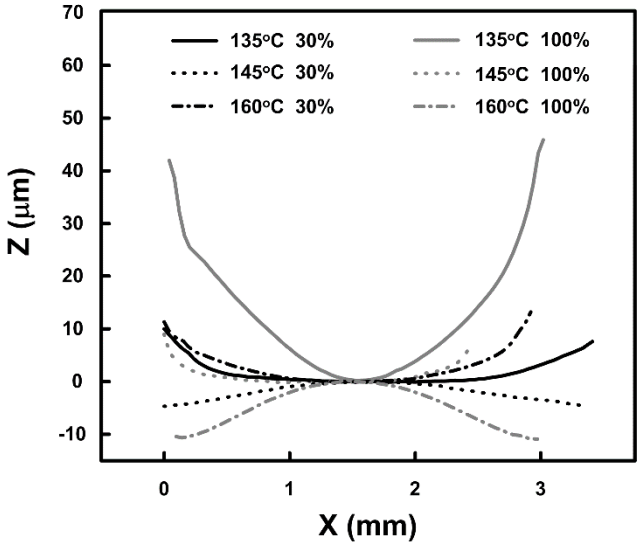

Figure 17. Comparison of typical cross-sections in samples programmed at 135 °C and above.

Further investigation is required to identify the actual mechanism behind above observed lens phenomenon in stretched samples.

4.3. Cracks

A PLμ Confocal Imaging Profiler with a magnification of 600 (thus, all scanned images are of the same size of 140 × 100 μm) was used to further examine the microscopic surface morphology of programmed samples.

Figure 18 presents typical surface morphology within necked area in the samples programmed at 128 °C to 30% and 100% programming strains. We can see many short straight-line type of micro-cracks, which are largely parallel and perpendicular to the direction of stretching, observed atop of both samples. Although the pattern of such cracks is not butterfly shaped as reported for a shape memory polystyrene in [29], the cross-sectional view of these cracks (bottom row of Figure 18) reveals the same kind of pile-up structure, which is due to the heating-responsive SME. On the other hand, there is no apparent crack formed in the non-naked area, as evidenced by Figure 19, for both programming strains.

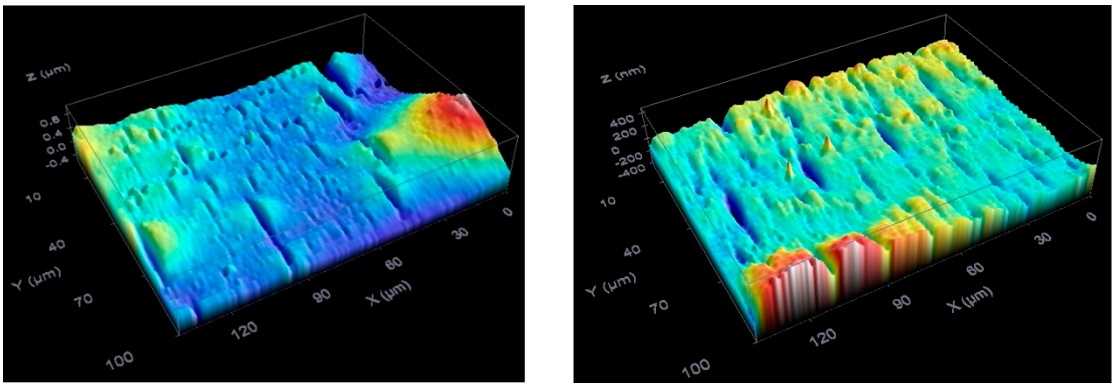

(**a1**) (**b1**)

Figure 18. *Cont.*

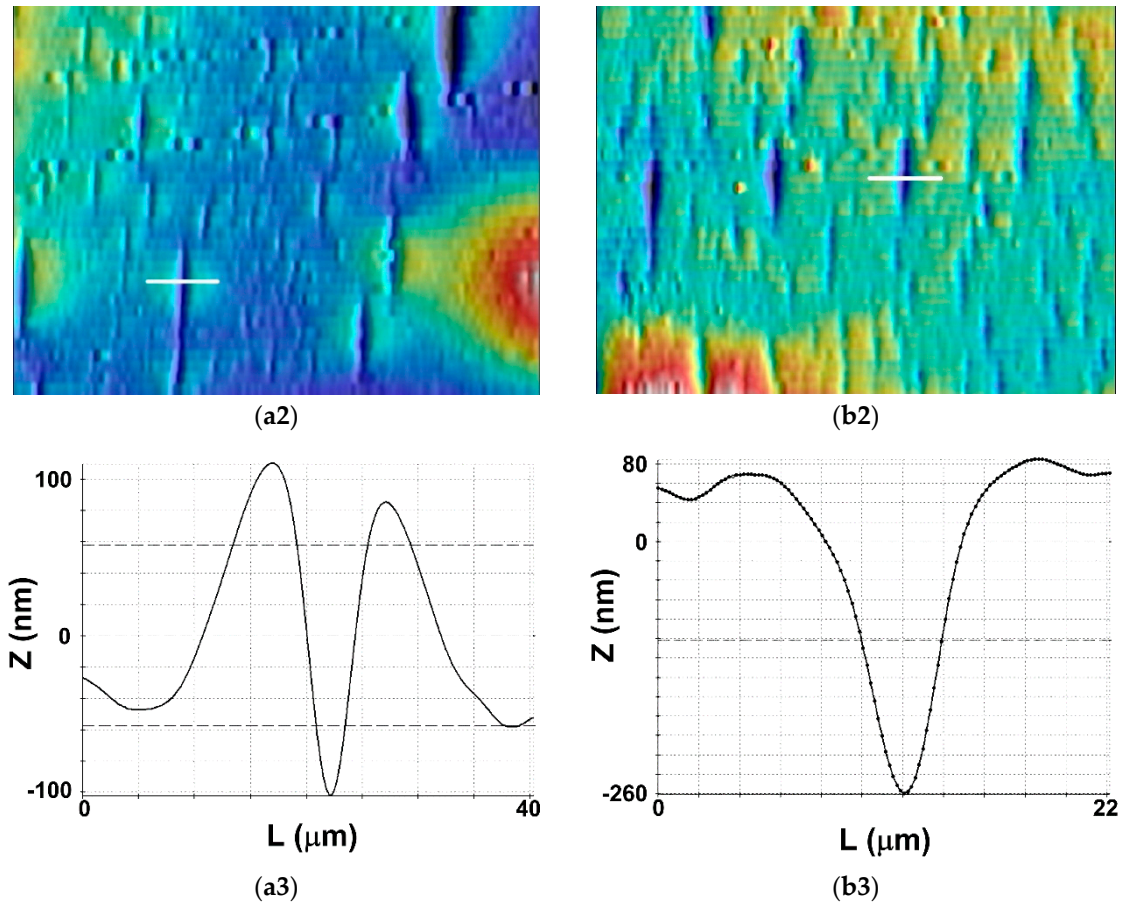

Figure 18. Typical surface morphology within necked area for samples programmed at 128 °C. Top row (1): 3D view; middle row (2): top view (area: 140 × 100 μm); bottom row (3) cross-section of the crack marked in middle row (2). Left: 30% strained; right: 100% strained.

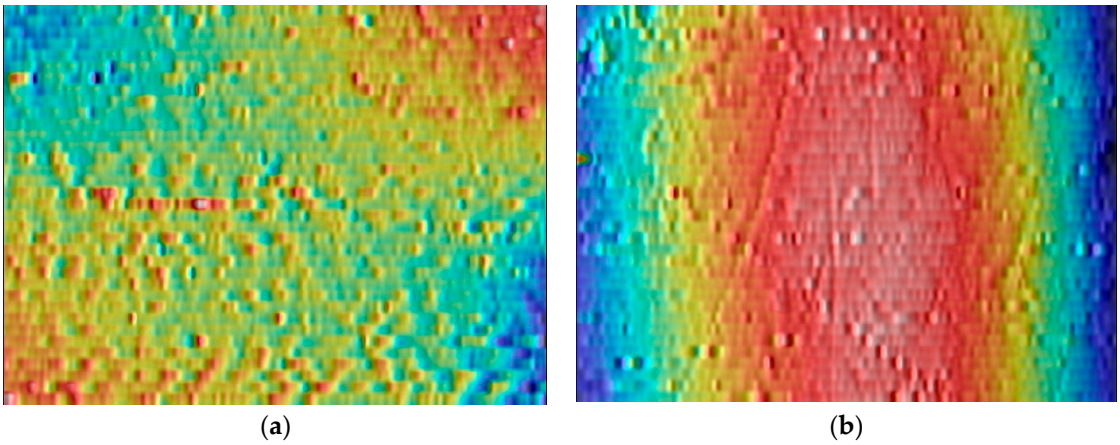

Figure 19. Typical surface morphology within non-necked area (140 × 100 μm). (**a**) 30% strained; (**b**) 100% strained.

For the samples programmed at 135 °C, same kind of parallel-line like cracks are only observed in the piece of sample programmed to 100% strain, as shown in Figure 20. There is no crack in the samples programmed at higher temperatures (namely 145 °C and 160 °C) regardless of the actual programming strain (Figure 21).

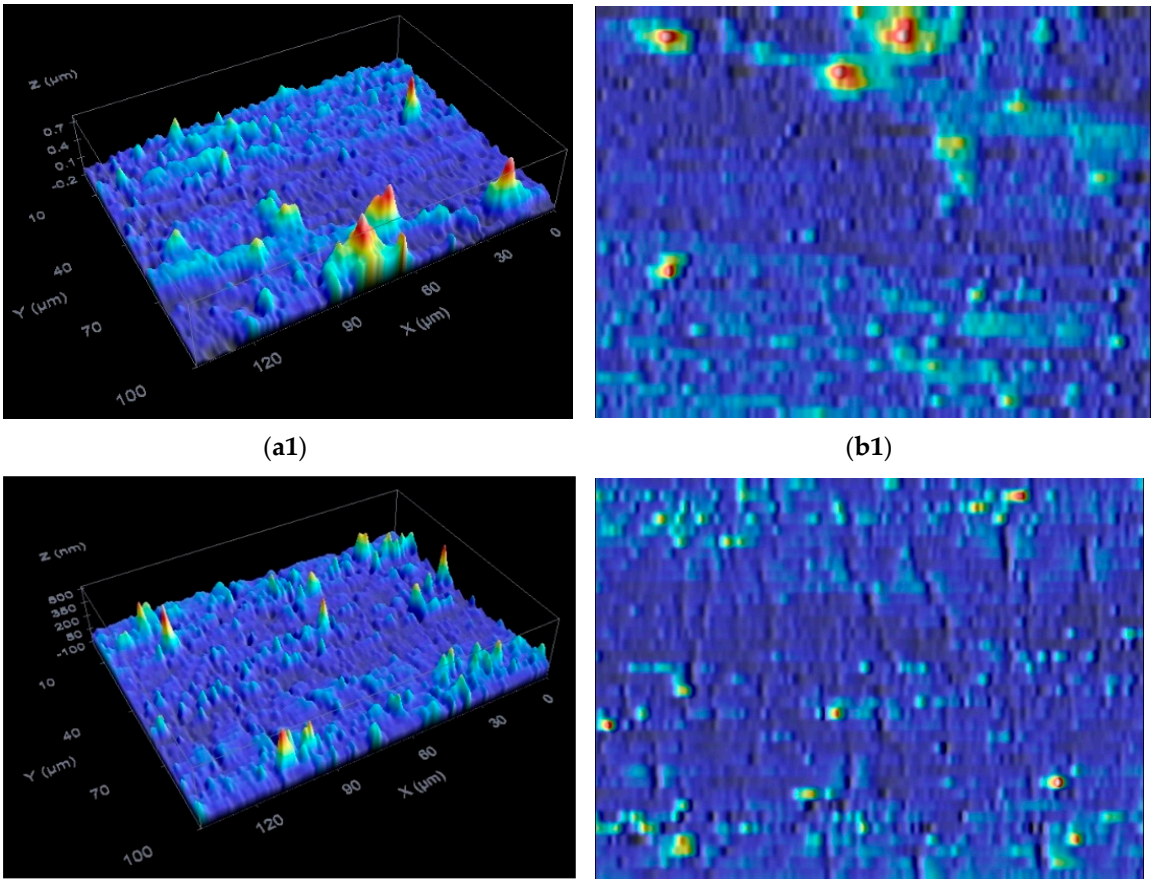

(**a1**) (**b1**)

(**a2**) (**b2**)

Figure 20. Typical surface morphology within the necked area in samples programmed at 135 °C. (**a**): 3D view; (**b**) top view. Top row (1): 30% strained; bottom row (2): 100% strained.

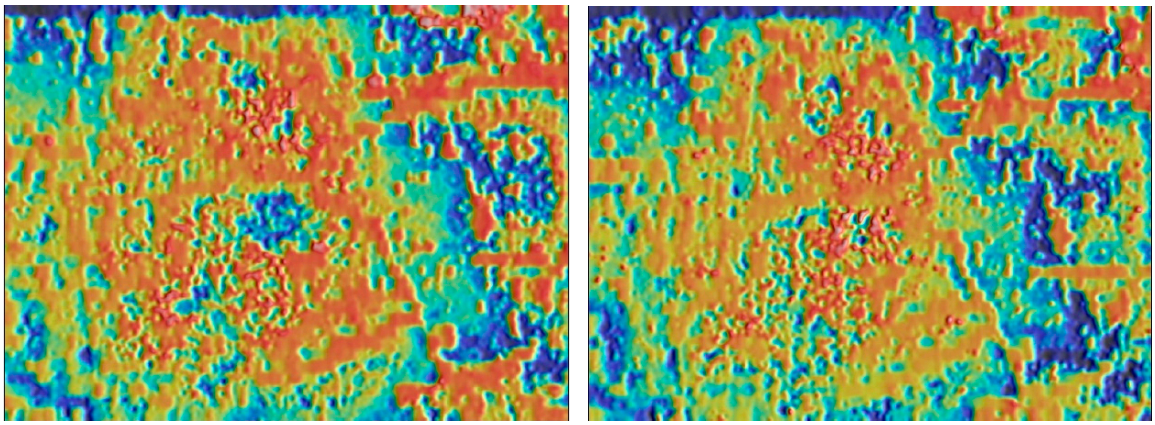

(**a1**) (**a2**)

Figure 21. *Cont.*

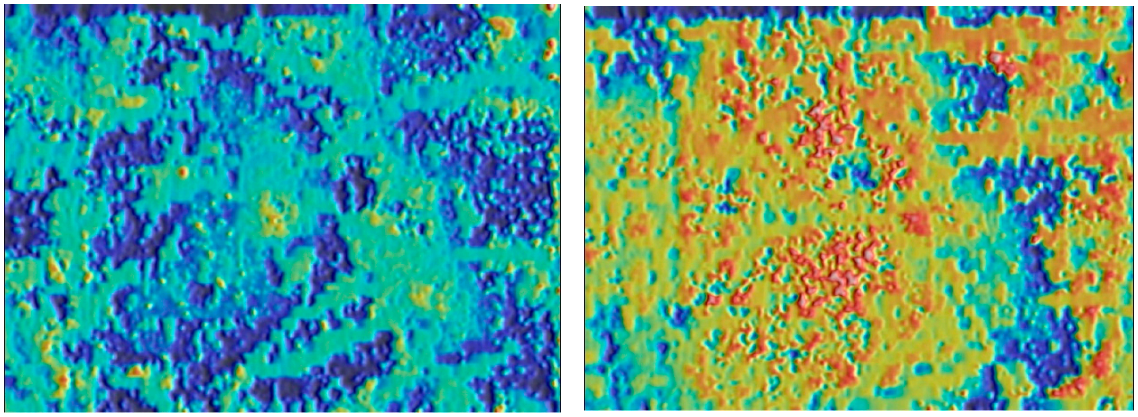

(**b1**) (**b2**)

Figure 21. Typical surface morphology (area: 140 × 100 μm) in samples programmed at 145 °C (**a**) and 160 °C (**b**). Left: 30% strained; right: 100% strained.

5. Further Discussion

In general, the PC material tested here has excellent heating-responsive SME. The maximum programming strain is limited to 25% at the most, if programming is conducted at room temperature.

However, as observed in Section 4, if the programming temperature is around the glass transition start temperature, micro-cracks may be found after programming by stretching. These micro cracks appear as short parallel lines and they are perpendicular to the direction of stretching, which is different from the butterfly pattern of cracks reported previously in a shape memory polystyrene [29]. These cracks are apparently due to the same kind of fracture in the relatively brittle areas of the material. As the cracks are short lines, and they should correspond to the brittle parts of the material, we expect that there is a network, which is relatively brittle (hard), within the sample. Because the applied programming temperature is around the glass transition start temperature, this network should be much denser than that reported in [29], in which the polystyrene was stretched close to its glass transition finish temperature (refer to the left column of Figure 22). Consequently, upon stretching, different crack patterns are observed as illustrated in the right column of Figure 22.

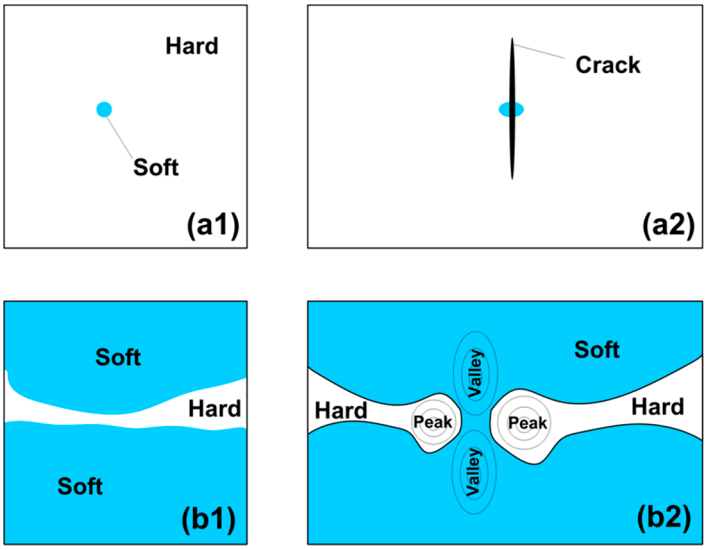

Figure 22. Formation of a short line crack (**a**) and a butterfly (**b**). Left (1): before stretching; right (2): after stretching.

Although these micro-cracks do not seemingly affect shape recovery of the material, its mechanical strength, in particular, under mechanical and/or thermo-mechanical cycling, is expected to be reduced.

On the other hand, if the applied programming temperature is over the glass transition temperature range, as revealed in Figure 10, together with a high programming strain, the capability for shape recovery of this material might be reduced. Since there is not any crack in the programmed sample (refer to Figure 21(b2)), the non-recoverable strain should be the result of permanent deformation in the elastic component/chain/segment [4].

Thus, the recommended programming temperature for this particular PC is within the middle of its glass transition range, i.e., around its T_g.

Necking, which occurs when the programming temperature is low, induces remarkable non-uniform deformation within the necking to non-necking transition area. Consequently, an elastic stress field in induced within this area. Furthermore, the necked area and non-necked area form concave and convex surfaces, respectively. It is also observed that, even without necking, the sample is programmed at high temperatures, the surface of the programmed sample is still most likely uneven. Most of the resulted surfaces are concave. Further systematical investigation is required before any conclusion can be drawn.

6. Conclusions

In this paper, we investigated the effects of programming temperature and maximum programming strain in the mode of uni-axial tension on the heating-responsive SME of a commercial PC and the surface features in programmed samples are examined.

Although excellent shape recovery upon heating to over the glass transition range is observed, it is found that a lower programming temperature around the glass transition start temperature results in many cracks in a short parallel line form, which is different from the butterfly pattern of cracks previously reported. On the other hand, programming at higher temperatures over the glass transition range may induce permanent deformation, if the programming strain is also higher.

Programming at low temperatures results in necking during stretching. Hence, non-uniform deformation within the gauge length area is observed, together with an elastic stress field within the necked to non-necked transition area. The surfaces of the necked and non-necked areas are concave and convex, respectively. Even for samples programmed at high temperatures without necking phenomenon, their surfaces are not flat.

It can be concluded that while the SME is a generic phenomenon for most polymers as pointed out in [4], the programming conditions should be carefully selected in order to achieve excellent shape recovery and in the meantime to avoid damage (such as cracks) to the material itself.

Acknowledgments: This project is partially supported by AcRF Tier 1 (RG172/15), Singapore, and the National Natural Science Foundation of China (No. 51303070). Z.G. Seow helped to conduct some of the experiments as part of his final year project.

Author Contributions: Xuelian Wu, Taoxi Wang, Weimin Huang and Yong Zhao conceived and designed the experiments; X. Wu, T. Wang and Y. Zhao performed the experiments; X. Wu and W. M. Huang analyzed the data; X. Wu and W. M. Huang wrote the paper.

Conflicts of Interest: The authors declare no conflict of interest.

References

1. Otsuka, K.; Wayman, C.M. *Shape Memory Materials*; Cambridge University Press: Cambridge, UK, 1998.
2. Huang, W.M.; Ding, Z.; Wang, C.C.; Wei, J.; Zhao, Y.; Purnawali, H. Shape memory materials. *Mater. Today* **2010**, *13*, 54–61. [CrossRef]
3. Wei, Z.G.; Sandstrom, R.; Miyazaki, S. Shape-memory materials and hybrid composites for smart systems —Part I Shape-memory materials. *J. Mater. Sci.* **1998**, *33*, 3743–3762. [CrossRef]

4. Huang, W.M.; Zhao, Y.; Wang, C.C.; Ding, Z.; Purnawali, H.; Tang, C.; Zhang, J.L. Thermo/chemo-responsive shape memory effect in polymers: A sketch of working mechanisms, fundamentals and optimization. *J. Polym. Res.* **2012**, *19*, 9952. [CrossRef]
5. Lendlein, A. *Shape-Memory Polymers*; Springer: Berlin, Germany, 2010.
6. Lendlein, A.; Kelch, S. Shape-memory polymers. *Angew. Chem. Int. Ed.* **2002**, *41*, 2034–2057. [CrossRef]
7. Zhao, Q.; Zou, W.; Luo, Y.; Xie, T. Shape memory polymer network with thermally distinct elasticity and plasticity. *Sci. Adv.* **2016**, *2*, e1501297. [CrossRef] [PubMed]
8. Kunzelman, J.; Chung, T.; Mather, P.T.; Weder, C. Shape memory polymers with built-in threshold temperature sensors. *J. Mater. Chem.* **2008**, *18*, 1082–1106. [CrossRef]
9. Behl, M.; Kratz, K.; Zotzmann, J.; Nochel, U.; Lendlein, A. Reversible bidirectional shape-memory polymers. *Adv. Mater.* **2013**, *25*, 4466–4469. [CrossRef] [PubMed]
10. Bothe, M.; Pretsch, T. Two-way shape changes of a shape-memory poly(ester urethane). *Macromol. Chem. Phys.* **2012**, *213*, 2378–2385. [CrossRef]
11. Salvekar, A.V.; Huang, W.M.; Xiao, R.; Wong, Y.S.; Venkatraman, S.S.; Tay, K.H.; Shen, Z.X. Water-Responsive Shape Recovery Induced Buckling in Biodegradable Photo-Cross-Linked Poly (ethylene glycol)(PEG) Hydrogel. *Acc. Chem. Res.* **2017**, *50*, 141–150. [CrossRef] [PubMed]
12. Mirtschin, N.; Pretsch, T. Designing temperature-memory effects in semicrystalline polyurethane. *RSC Adv.* **2015**, *5*, 46307–46315. [CrossRef]
13. Zhou, J.; Turner, S.A.; Brosnan, S.M.; Li, Q.; Carrillo, J.-M.Y.; Nykypanchuk, D.; Gang, O.; Ashby, V.S.; Dobrynin, A.V.; Sheiko, S.S. Shapeshifting: Reversible shape memory in semicrystalline elastomers. *Macromolecules* **2014**, *47*, 1768–1776. [CrossRef]
14. Kagami, Y.; Gong, J.P.; Osada, Y. Shape memory behaviors of crosslinked copolymers containing stearyl acrylate. *Macromol. Rapid Commun.* **1996**, *17*, 539–543. [CrossRef]
15. Wang, L.; Di, S.; Wang, W.; Chen, H.; Yang, X.; Gong, T.; Zhou, S. Tunable temperature memory effect of photo-cross-linked star PCL–PEG networks. *Macromolecules* **2014**, *47*, 1828–1836. [CrossRef]
16. Zhu, Y.; Hu, J.L.; Luo, H.S.; Young, R.J.; Deng, L.B.; Zhang, S.; Fan, Y.; Ye, G. Rapidly switchable water-sensitive shape-memory cellulose/elastomer nano-composites. *Soft Matter* **2012**, *8*, 2509–2517. [CrossRef]
17. Wu, X.L.; Huang, W.M.; Ding, Z.; Tan, H.X.; Yang, W.G.; Sun, K.Y. Characterization of the thermoresponsive shape-memory effect in poly(ether ether ketone) (PEEK). *J. Appl. Polym. Sci.* **2014**, *131*, 39844. [CrossRef]
18. Wu, X.L.; Huang, W.M.; Seow, Z.G.; Chin, W.S.; Yang, W.G.; Sun, K.Y. Two-step shape recovery in heating-responsive shape memory polytetrafluoroethylene and its thermally assisted self-healing. *Smart Mater. Struct.* **2013**, *22*, 125023. [CrossRef]
19. Wu, X.L.; Huang, W.M.; Tan, H.X. Characterization of shape recovery via creeping and shape memory effect in ether-vinyl acetate copolymer (EVA). *J. Polym. Res.* **2013**, *20*, 150. [CrossRef]
20. Zhang, J.L.; Huang, W.M.; Lu, H.B.; Sun, L. Thermo-/chemo-responsive shape memory/change effect in a hydrogel and its composites. *Mater. Des.* **2014**, *53*, 1077–1088. [CrossRef]
21. Wong, Y.S.; Vijay, S.A.; Da Zhuang, K.; Liu, H.; Birch, W.R.; Tay, K.H.; Huang, W.M.; Venkatraman, S.S. Bioabsorbable radiopaque water-responsive shape memory embolization plug for temporary vascular occlusion. *Biomaterials* **2016**, *102*, 98–106. [CrossRef] [PubMed]
22. Wang, T.X.; Huang, W.M.; Aw, J.E.; He, L.W.; Vettorello, M. Comfort fitting using shape memory polymeirc foam. *J. Test. Eval.* **2017**, *45*, 12. [CrossRef]
23. Zhao, Y.; Huang, W.M.; Fu, Y.Q. Formation of micro/nano-scale wrinkling patterns atop shape memory polymers. *J. Micromech. Microeng.* **2011**, *21*, 067007. [CrossRef]
24. Zhao, Y.; Wang, C.C.; Huang, W.M.; Purnawali, H.; An, L. Formation of micro protrusive lens arrays atop poly(methyl methacrylate). *Opt. Express* **2011**, *19*, 26000–26005. [CrossRef] [PubMed]
25. Ecker, M.; Pretsch, T. Durability of switchable QR code carriers under hydrolytic and photolytic conditions. *Smart Mater. Struct.* **2013**, *22*, 094005. [CrossRef]
26. Salvekar, A.V.; Zhou, Y.; Huang, W.M.; Wong, Y.S.; Venkatraman, S.S.; Shen, Z.; Zhu, G.; Cui, H.P. Shape/temperature memory phenomena in un-crosslinked poly-ε-caprolactone (PCL). *Eur. Polym. J.* **2015**, *72*, 282–295. [CrossRef]

27. Lu, H.; Huang, W.M.; Wu, X.L.; Ge, Y.C.; Zhang, F.; Zhao, Y.; Geng, J. Heating/ethanol-response of poly methyl methacrylate (PMMA) with gradient pre-deformation and potential temperature sensor and anti-counterfeit applications. *Smart Mater. Struct.* **2014**, *23*, 067002. [CrossRef]
28. Wu, X.L.; Huang, W.M.; Lu, H.B.; Wang, C.C.; Cui, H.P. Characterization of polymeric shape memory materials. *J. Polym. Eng.* **2017**, *37*, 1–20. [CrossRef]
29. Liu, N.; Huang, W.M.; Phee, S.J. A secret garden of micro butterflies: Phenomenon and mechanism. *Surf. Rev. Lett.* **2007**, *14*, 1187–1190. [CrossRef]